The role of a split injection strategy in the mixture formation and combustion of diesel spray:

Hadadpour, Ahmad; Jangi, Mehdi; Pang, Kar Mun; Bai, Xue Song

[Link to publication on Research at Birmingham portal](#)

The role of a split injection strategy in the mixture formation and combustion of diesel spray: A large-eddy simulation

Ahmad Hadadpour[a], Mehdi Jangi[b,*], Kar Mun Pang[c], Xue Song Bai[a]

[a] Division of Fluid Mechanics, Department of Energy Science, Lund University, P.O. Box 118, S 221 00 Lund, Sweden
[b] Department of Mechanical Engineering, School of Engineering, University of Birmingham, Edgbaston, Birmingham, B15 2TT
[c] Department of Mechanical Engineering, Technical University of Denmark, 2800 Kgs. Lyngby, Denmark

Abstract

The role of a split injection in the mixture formation and combustion characteristics of a diesel spray in an engine-like condition is investigated. We use large-eddy simulations with finite rate chemistry in order to identify the main controlling mechanism that can potentially improve the mixture quality and reduces the combustion emissions. It is shown that the primary effect of the split injection is the reduction of the mass of the fuel-rich region where soot precursors can form.

Furthermore, we investigate the interaction between different injections and explain the effects of the first injection on the mixing and combustion of the second injection. Results show that the penetration of the second injection is faster than that of the first injection. More importantly, it is shown that the ignition delay time of the second injection is much shorter than that of the first injection. This is due to the residual effects of the ignition of the first injection which increases the local temperature and maintains a certain level of combustion some intermediates or radical which in turn boosts the ignition of the second injection.

Keywords:
Split injection, Jet-jet interaction, Mixture formation, Large-eddy simulation

---

*Corresponding author.
E-mail address: mehdi.jangi@energy.lth.se

1. Introduction

Multiple-injection strategies are widely used in combustion engine applications for a variety of reasons, for example, improved combustion efficiency [1], emission of unburned hydrocarbons (UHC) [2], nitrogen oxides (NO_X) [3], soot [4], and engine noises [5]. There is a general agreement on the beneficial effects of using an optimized split injection on the improvement of engines performance [6–8]. However, the underlying physical processes that need to be considered for such an optimization are not fully understood [8] and this might lead to the use of some strategies which are not optimum or even have advert effects. For instance, chen showed that a pre-injection strategy, in which an injection splits into a short first injection and a long second injection, can reduce the NO_X, CO, UHC emissions, whereas it increases the soot emission by using multiple injection [6]. As another example, Chartier et al. [9] showed that a double injection can be beneficial on the reduction of UHC if only the single injection splits into a large first injection and a small post-injection.

In lights of this, the focus of the current study is on the understanding of mechanisms by which a split injection changes the combustion of a diesel spray. The suggested explanations for the effects of split injection in the literature can be categorized into three main mechanims [8]: (i) the split injection enhances the mixing and it reduces the local equivalence ratio and improves premixing before the start of high-temperature combustion [10–12]. In this work, we call this mechanism the equivalence ratio effects, and it will act in favor of reducing the rate of soot formation. In the same context, some authors suggested that this mechanism can also increase the soot oxidation rate, as an improving premixing provides a better fresh oxygen in the reaction zone [8]; (ii) the second mechanism indicates that the heat release from the second injection increases the temperature of combustion and it affects soot formation and oxidation. Hereby, we call this mechanism the temperature effects [13–16]; (iii) finally, some authors suggested that a split injection as such does not change the nature of combustion, and each injection should be considered as a stand-alone spray combustion [17–20]. The only controlling factor is the injection duration which is shorter when a single injection splits into multiple injections. This concept is called "split-flame" [8, 18]. We call this mechanism the injection duration effects. This mechanism relies on the fact that soot formation is related to the duration of each injection, and the longer is the injection duration the more is the soot emission.

Depending on the major controlling mechanism, an injection can be optimized to achieve the best combustion emission behavior. However, this requires identifying which of the above-mentioned mechanisms, has the major contribution to the mixture formation and ignition of a diesel spray in an engine like condition. The current work investigates the effects of splitting a single injection into two injections with an equal total injected fuel. The condition and setup are chosen based on an experiment that is available in the Engine Combustion Network (ECN) website [21]. The main questions that are seeking to answer in this paper are: whether a split injection primarily changes the local combustion temperature or the local equivalence ratio? whether two consecutive injections interact with each other or they are burning as a separate spray combustion? And if they are interacting in what way the first injection can change the combustion of the second injection. Finally, we explore the tendency of soot formation in single and double injections.

2. Mathematical model

Since double injection spray flame is a transient phenomenon that involves large-scale coherent flow, and multiple combustion modes (ignition, premixed flame and diffusion flames), we chose to use a high fidelity numerical model, large-eddy simulation based on direct coupling of detailed chemistry. Favre-filtered LES conservation equations for the gas phase can be written as:

$$\frac{\partial \overline{\rho}}{\partial t} + \frac{\partial \overline{\rho}\tilde{u}_j}{\partial x_j} = \overline{S_\rho^s}, \tag{1}$$

$$\frac{\partial \overline{\rho}\tilde{u}_i}{\partial t} + \frac{\partial}{\partial x_j}[\overline{\rho}\tilde{u}_i\tilde{u}_j - \overline{\tau}_{ij} + \tau_{ij}^{sgs}] = \overline{S_{u_i}^s} \tag{2}$$

$$\frac{\partial \overline{\rho}\tilde{h}}{\partial t} + \frac{\partial \overline{\rho}\tilde{u}_j\tilde{h}}{\partial x_j} - \frac{\partial}{\partial x_j}\left[\overline{\lambda}\frac{\partial \tilde{T}}{\partial x_j} + h_j^{sgs}\right] = \overline{S_h^s} \tag{3}$$

The overline denotes the general filtering and tilde denotes the Favre filtering. u is velocity, h is enthalpy and $\overline{S_\rho^s}$, $\overline{S_{u_i}^s}$, $\overline{S_h^s}$ are source terms that account for the exchange rate of the mass, momentum and heat between the gas and liquid phases, respectively. $\overline{\tau}_{ij}$ is filtered stress tensor obtained from the resolved strained rate. Superscript s denotes the spray and sgs denotes the subgrid variables. τ^{sgs}, h^{sgs}, and ϕ^{sgs} are subgrid stress, heat and species mass fluxes.

Closures for spray source terms $\overline{S_\rho^s}$, $\overline{S_{u_i}^s}$, $\overline{S_h^s}$ are obtained using Lagrangian particle tracking (LPT) approach. In this approach, a spray is considered as discrete phase consisting of a large number of evaporating

droplets. Each droplet should be tracked individually in a Lagrangian framework. The number of droplets in real sprays is massively large, thus, tracking every single droplet is not computationally feasible. The efficient way is to describe the spray as a limited number of parcels within which the droplets have identical properties, e.g., diameter and temperature. Lagrangian tracking is performed for parcels instead of individual droplets. Equations of motion for parcels are [22]:

$$\frac{d}{dt}\mathbf{x_p} = \mathbf{u_p} \qquad (4)$$

$$\frac{d}{dt}\mathbf{u_p} = \frac{C_D}{\tau_p}\frac{Re_p}{24}(\mathbf{u_g} - \mathbf{u_p}) = \frac{C_D}{\tau_p}\frac{Re_p}{24}\mathbf{v_{rel}} \qquad (5)$$

Re_p is the parcel Reynolds number defined as $Re_p = \rho_g|\mathbf{v_{rel}}|\,d_p/\mu_g$ with d_p being the parcel diameter and μ_g gas-phase viscosity. C_D is the drag coefficient and is modelled as $C_D = \frac{24}{Re_p}(1 + \frac{1}{6}Re_p^{2/3})$ for $Re_p < 1000$ and $C_D = 0.424$ for $Re_p >= 1000$. $\mathbf{x_p}$ is the parcel vector position, $\mathbf{u_p}$ is the parcel velocity, $\mathbf{u_g}$ is the surrounding gas velocity and $\mathbf{v_{rel}}$ is the relative velocity between the parcel and surrounding gases. $\tau_p = \rho_l d_p^2/18\rho_g\nu_g$ is the parcel characteristic time. For more details about the Eulerian-Lagrangian approch see Ref. [23].

To obtain a closed form for the filtered source terms due to the elementary reactions in the species transport and energy equations the so-called partially-stirred reactor (PaSR) approach is used. This approach is suitable when the combustion process is ignition-driven. The use of this method has been validated in our previous work [24]. The chemistry coordinate mapping (CCM) approach is used to accelerate the simulation. For more details about this approach see Ref. [25]. The used kinetic mechanism has 54 species and 269 reactions. Further details about it can be found in Ref. [26].

In addition to Eqs. 1-3, two additional equations are solved in order to track the evolution of each injection and its contribution in the local mixture fraction as below:

$$\frac{\partial\overline{\rho}\tilde{Z}_i}{\partial t} + \frac{\partial\overline{\rho}\tilde{u}_j\tilde{Z}_i}{\partial x_j} - \frac{\partial}{\partial x_j}\left[\overline{\rho D}\frac{\partial\tilde{Z}_i}{\partial x_j} + \Phi_{Z_i}^{sgs}\right] = \overline{S_{Z_i}^s} \qquad (6)$$

where Z_i is the mixture of the i-th injection. $\overline{S_{Z_i}^s}$ is the source term of the mass exchange rate for the i-th injection, and that takes the value of $\overline{S_\rho^s}$ during the i-th injection, and become zero after the end of that injection. The total mixture fraction Z is then equal to the sum of Z_is. The local equivalence ratio ϕ can be calculated as $\phi = [Z/(1-Z)]/[Z/(1-Z)]_{st}$. In addition, the local equivalence ratio of each of injections are defined

and calculated as $\phi_i = [Z_i/(1-Z_i)]/[Z/(1-Z)]_{st}$. In this way, the contribution of the injected mass from each injection on the local equivalence ratio can be determined.

OpenFOAM is used for numerical solution of the governing equations. Both temporal and spatial terms were discretized using implicit second-order schemes.

3. Results and discussion

3.1. Case specification

The baseline case in this study is chosen based on experiments by Scott et al. [27] where a spray of n-dodecane was injected through a 90 μm injector into a pressurized and preheated constant volume vessels. The vessel was nearly cubical and has a volume of approximately 1 liter. The initial temperature and pressure of the gases in the vessel were 900 K and 6 MPa, respectively, and the fuel temperature was 363 K. These thermodynamic conditions are similar to the in-cylinder conditions of modern compression-ignition engines [28]. In the experiment, a double injection with a duration of 0.5 ms for each injection, and a dwell time of 0.5 ms was used. The setting of our simulations is based on this experimental condition. In addition to this case, we performed a simulation for a 1 ms single injection case, in which the total injected fuel is same as that in double injection case. Apart from the difference in the injection strategy, all other conditions and setting are the same for both cases. The computational domain for both cases is a cubical vessel of 108 $mm \times$ 108 $mm \times$ 108 mm, similar to that in the experiment. This domain was discretized using 1.7 million cells using a uniform Cartesian mesh with two refinement level. The mesh refinements performed inside two cylinders with a diameter of 24 mm and 16 mm along the centreline of the injector (See Fig. 1). The mesh resolution inside the refinement region is 0.24 mm. In addition to the validation of the simulation in this work which will be present in next section, this setting was used and validated in our previous publication [23]

3.2. Validation of the simulation

Figure 2a shows the pressure-rise history in the vessel for the double injection cases. As it can be seen, the simulation results agree well with the experimental data. In particular, the increase in the pressure-rise-rate after the start of the second injection at $t = 1\ ms$ has been reproduced well. Fig. 2b shows the apparent heat release rate (AHRR) curves. Except for the oscillation at the early times, the simulation results during and after the injection agree well with the experimental data.
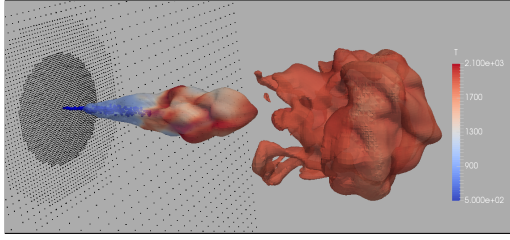
Figure 1: The iso-surface of Z_1 and Z_2, coloured by temperature. Small spheres near the injector are Lagrangian particles of fluid fuel. Two mesh refinement region, as explained in the text can be seen in the computational domain.

The peaks at $t = 0.62\ ms$, and $t = 1.58\ ms$ are attributed to the heat release from the first and the second injections and have been over-predicted by approximately $0.1\ ms$ compared to those of the experiments. The same over-prediction can be seen for the ignition delay time based on the pressure-rise-rate in the experiment and in the simulation, which are $0.33\ ms$ and $0.41\ ms$, respectively. However, it is worth mentioning that according to the ECN website, the reported ignition delay of the single injection ECN spray A at the same ambient conditions as those of current experiments is $0.39\ ms$ [21], which is quite close to the current prediction results in the simulation.

Figure 3 shows the vapor penetration of the double injection case. As mentioned in section 2, two extra transport equations are solved to trace each of the injections. This allows us to study the penetration of each injection, separately. In Fig. 3, the solid line is the penetration length based on the total mixture fraction Z. As it can be seen in this figure, the vapor penetration agrees well with the measurement. The dashed line is the penetration based on Z_2, and the dash-dotted line is the time-shifted penetration curve based on Z_2 which is shifted 1 ms toward the left-hand side of the chart. Interestingly, it can be seen that the penetration of the second injection is much faster than that of the first injection. This can be understood by comparing the slope of the solid line with that of the dash-dotted curve. This is essentially attributed to the history effects of the first injection and its residual effect which makes the penetration of the second injection faster owing due to the fact that the ambient gases have a non-zero momentum in the direction of injection once the second injection emerges into the domain, whereas it was not the case for the first injection.

Since the tip of the second injection travels faster than that of the first injection, it reaches the tip of the first injection at $t = 2.24\ ms$. This observation is important because it shows that the second injection overlaps and
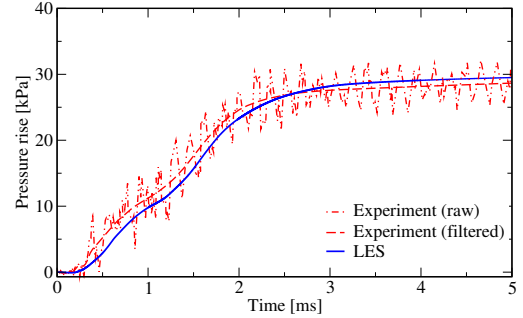
(a)
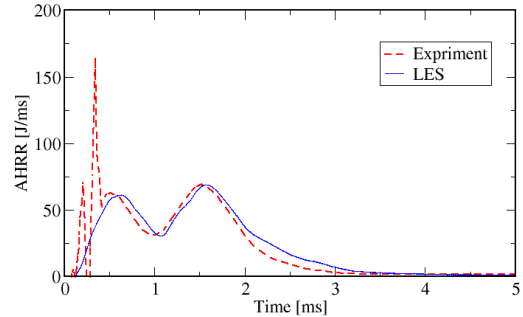
(b)

Figure 2: (a) Measured pressure trace in the experiment [27] and LES for double injections case; (b) Apparent heat release rate (AHRR) for the same case.

interacts with the first injection, even for this case where the dwell period is relatively large (0.5 ms). Especially, this result disagrees with the mechanism-iii discussed earlier in the introduction section. Apparently, results show that in current setting two injections do interact with each other, and cannot be considered as two stand-alone injections. We will come back to this point in the next section and provide further evidence on the effects on the first injection of the ignition and combustion of the second injection.

3.3. The role of split injection on the mixture formation

It is known that the soot behavior of a diesel spray combustion is strongly linked to the local equivalence ratio of the mixture and its temperature. It has been suggested that in engine applications with hydrocarbon fuels, the formation of soot occur when the local equivalent ratio (ϕ) of the reactants is greater than 2 and their temperature is within the range of 1600-2300 K [30–32]. While it is understood that these values are not precise and soot can be observed outside of this range, it is qualitatively justifiable to use this range as a representative region for soot formation. Hereinafter, this $\phi - T$ range is referred to as the "soot-zone".
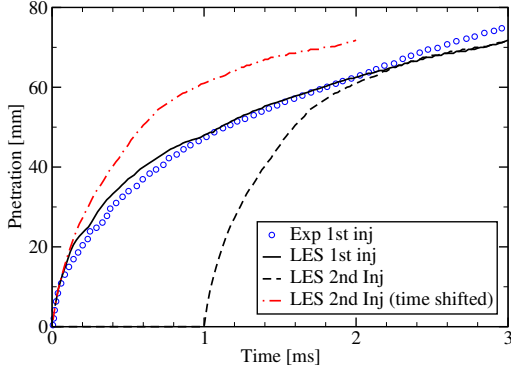
4

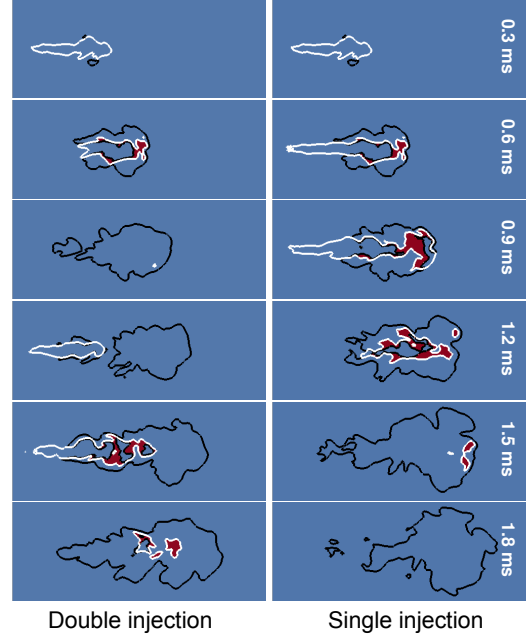Figure 3: Vapor-penetration of fuel in the reacting double injection case in the experiment [27] and LES.

Figure 4: The soot formation zone in the the double injections and single injection along the time after start of injection (ASI). The white line is iso-contour of $\phi = 2$. The black line is iso-contour of $T = 1600$K. The red zone (darker zone in the grey scale print) is where $\phi > 2$ and 1600 K$ < T <$ 2300 K. Each frame shows $70mm \times 28mm$

Figure 4 shows the snapshots of the "soot-zone" for single and the double injection cases at different times. The white line is the iso-contour of $\phi = 2$, and the region confined by this boundary shows the fuel-rich region where the equivalence ratio of the gases are sufficiently large for soot formation. The black line is iso-contour of $T = 1600K$. Since for all instances shown in this figure the maximum temperature is below $T = 2300K$, the region inside the black line boundary depicts the gases with sufficient temperature for soot formation. The region filled in red/dark color shows the "soot-zone" in which both equivalence ratio and temperature of the reactants are within the region that soot can form, i.e. $\phi > 2$ and 1600 K$ < T <$ 2300 K.

The end of the first injection is at 0.5 ms, therefore in Fig. 4 the results at $t = 0.3\ ms$ for both single and double injections cases are the same. At this time the first igniting sites can already be identified in the peripheral region of the flow in the shear layer. At this instance, although the equivalence ratio is sufficiently high, the reactant temperature is still not enough to form soot. At $t = 0.6\ ms$, the local temperature in both cases have increased, and a significantly large "soot-zone" can be identified; however, in the center of the flow along the spray axis, the temperature is still below the range of soot formation range. Note that at this instant for the single injection case the fuel is still injecting, whereas the first injection of the double injection case has finished and the injection is paused. The effect of the injection pausing in the double injection case can be clearly seen by comparing the iso-contour of $\phi = 2$ for two cases. Nonetheless, in terms of the "soot-zone", both cases are almost identical at this instance and the effects of the split injection on "soot-zone" become more evident at the later time, e.g., at $t = 0.9\ ms$, and $t = 1.2\ ms$. It can be seen that the "soot-zone" of the double injec-

tion case in these instances is much smaller than that of the single injection case. The results at $t = 1.2\ ms$ are important as they show the effects of the air entrainment due to the injection pausing which in turn improves the premixing and reduces the "soot-zone" in this case. This finding is consistent with the literature [29, 33].

The important observation is that at this instance, while the region with sufficient temperature for soot formation is relatively large for both cases, the main difference in them is the smaller fuel-rich area for the double injection case. Therefore, results show that in this instance, it is the equivalence ratio effect (mechanism-i) that is responsible for reducing the "soot-zone" rather than the temperature effects (mechanism-ii). We further examine these in order to identify the major controlling mechanism and confirm the dominant mechanism.

Fig. 5 shows the normalized mass of the gases of the "soot-zone" (the region filled in red in Fig. 4) for each case in the entire computational domain. Furthermore, the normalized mass of the gasses with a temperature within the range of 1600-2300 K (the region inside the black line in Fig. 4), as well as the normalized mass of the gases with $\phi > 2$ (the region inside the white line in 4) are shown. As it can be seen, in both cases after a short period from the start of ignition, the mass of the

temperature range 1600-2300 K rapidly increases and it is affected by the split injection, only moderately. This is not the case, however, for the mass of the region with $\phi > 2$. It is clearly seen that the mass of this region has been largely reduced in the split injection case. All these indicate that the "soot-zone" is not affected by the temperature effects (mechanism-ii), and it is essentially controlled by the equivalence ratio effects (mechanism-i).
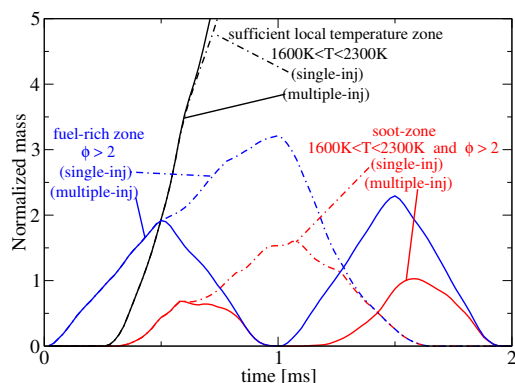

Figure 5: The solid lines are results from the double injection case and the dash-dotted lines are from the single injection case. The black lines are the normalized mass of the gases with a temperature within the "soot-zone" range, 1600 K < T < 2300 K. The blue lines are the normalized mass of gasses with a equivalence ratio within the "soot-zone", $\phi > 2$. The red lines are the mass of the "soot-zone" which is defined as as 1600K< T <2300K and $\phi > 2$. The vertical axis, mass, is normalized by the total mass of fuel which is 3.7 mg.

Another interesting observation in Fig. 4 is the growth of the "soot-zone" after t = 1.5 ms for the double injection case. This is a consequence of the second injection which creates a new "soot-zone"; however, the mass of such zone is much smaller than that of the single injection case. This is manifested in the results shown in Fig. 5, and considering the fact that the total mass of the "soot-zone" in the double injection case is always much smaller than the single injection case. Also, the results and discussion here can explain the typical role of pre-injection strategies in increasing the soot emission reported in Refs [6, 27].

3.4. Jet-jet interaction in split injection

The mechanism-iii describes consecutive injections as two separate spray combustion and suggests that different injections do not interact with each other. In this section, we examine this hypothesis by analyzing the results from the double injection case. It can be seen in Fig. 4 and at t=1.2 ms, which is only 0.2 ms after the start of the second injection, that the injected fuel from the second injection has already experienced in

some levels of high-temperature combustion. This is understood by considering the isocontour of T = 1600 K (shown in black near the nozzle) and comparing it with the results of the single injection case on the same figure. Considering the fact that the ignition delay time of the n-dodecane at the conditions of the current problem is about 0.4 ms, these results imply that the first injection has a great impact on the ignition and combustion of the second injection by shortening the ignition delay of the second injection. Obviously, this dismisses the mechanism-iii, at least under the conditions of the current study.

There are at least two ways that the first injection can change the combustion of the second injection: (a) the residual radicals and intermediates from the ignition processes of the first injection increases the reactivity of the near-nozzle region. In this way, the second injection is actually passed through an ambient that is chemically highly reactive, thereby the ignition delay time of the second injection decreases; (b) the penetration of the second injection is enhanced because of the residual momentum effects of the first injection as it was discussed before. Therefore the fuel from the second injection enters into the reaction zone of the first injection. Depending on the time after the start of the second injection and the dwell period, both processes can occur. We further investigate the results to provide a better understanding of the underlying physical processes.

Figure 6 shows snapshots of the mass fraction of hydroxyl (Y_{OH}) radical for double injection case in the interval of 1.1-1.4 ms. Y_{OH} is used to identify the location of the reaction zone. The iso-contour of ϕ_2 = 1 (see Eq. 6, and the definition of ϕ_2 therein) is also shown to identify the location of the second injection. Shown in black on these snapshots is the iso-contour of T = 1600 K. In the first snapshot at 1.1 ms, which is only 0.1 ms after the start of the second, the tip of the second injection reaches the high-temperature region of the first injection. This is due to a fast penetration of the second injection as discussed in previous sections, also due to the propagation of the lift-off toward the nozzle, after the end of the first injection. The second injection undergoes a significant self-ignition process as it was confirmed by examining the distribution of Y_{HO2} and other intermediates (not shown). This indicates that ignition-boosting effect of the first injection is important during the early injection period of the second injection. However, as soon as the second injection reaches the high-temperature region of the first injection in the later time, the fuel from the second injection is immediately ignited. This can be confirmed by considering the distribution of a thin Y_{OH} layer across the iso-contour

$\phi_2 = 1$, as it can be seen in the results from times 1.3-1.4 ms, which exhibits the typical characteristic of a non-premixed flame in that region. The effect of enhanced penetration of the second injection by the trace momentum left from the first injection certainly speed up the ignition of the second injection.
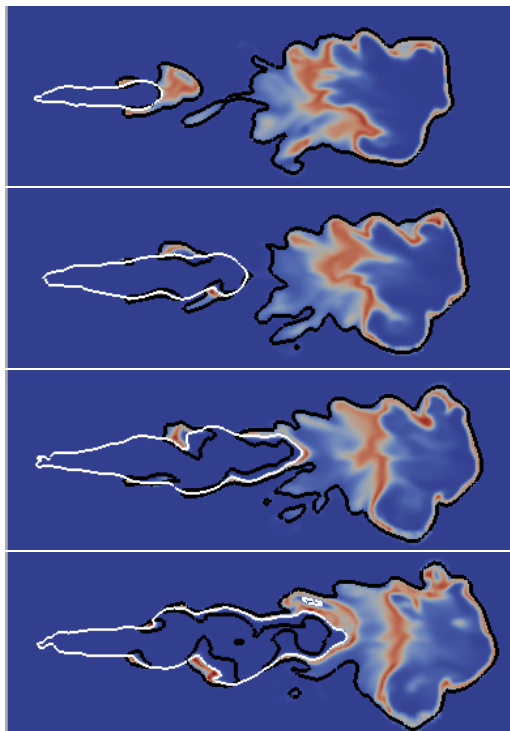

Figure 6: Snapshots of mass fraction of hydroxyl radicals, Y_{OH}, in the double injection case t=1.1-1.4 ms ASI; the interval between snapshots is 0.1 ms; The white line is iso-contour of $\phi_2 = 1$, and the black line is iso-contour of $T = 1600$ K. Each frame shows a $55mm \times 20mm$ domain

Conclusion

An LES coupled with LPT was performed to study the effects of a split injection on the mixture formation and combustion behavior of an n-dodecane diesel spray in a pressurized constant volume vessel at engine-like conditions. Two extra transport equations were introduced and solved in order to track the time history of different injections and their contribution in the local mixture fraction. Simulation results were compared with the experimental data and reasonable agreements were achieved. The results were further analyzed to identify the role of the split injection on the local and temporal distribution of the equivalence ratio and temperature. The main focuses of this study were to identify the major mechanisms that can potentially lead to the reduction of soot formation, and also to understand the interaction between two consecutive injections.

It was shown that the primary reason that soot formation zone is restricted in double injection strategies is due to the decrease of the local equivalence ratio. Especially, it was shown that such enhancements lead to the reduction of the mass of the regions where the equivalence ratio is large enough to form soot precursors. It is also shown that the penetration and combustion of the second injection are significantly modified by the first injection, which supports the idea that the two consecutive injections can largely interact with each other. In particular it is shown that: (1) the penetration rate of the second injection is much faster than the first injection; (2) the ignition delay time of the second injection is much shorter than the first; (3) the injected fuel of the second injection can catch up with that of the first injection, and at some point the ignition of the second injection will interact with the reaction front of the first injection. Such interaction will likely form a combustion system that involves auto-ignition, premixed flame propagation, and non-premixed flame combustions. Further analysis is required to fully understand such interactions and their impacts on the overall combustion and emissions behavior of a diesel spray combustion in engines.

Acknowledgments

References

[1] A. A. Moiz, M. M. Ameen, S.-Y. Lee, S. Som, Combustion and Flame 173 (2016) 123–131.

[2] J. O'Connor, M. Musculus, SAE International Journal of Engines 6 (2013) 379–399.

[3] T. Tow, D. Pierpont, R. D. Reitz, SAE Technical Paper (1994).

[4] R. Hessel, R. D. Reitz, M. Musculus, J. O'Connor, D. Flowers, SAE International Journal of Engines 7 (2014) 694–713.

[5] S. Mendez, B. Thirouard, SAE International Journal of Fuels and Lubricants 1 (2008) 662–674.

[6] S. K. Chen, SAE Technical Paper (2000).

[7] M. Dürnholz, H. Endres, P. Frisse, SAE Technical Paper (1994).

[8] J. O'Connor, M. Musculus, SAE International Journal of Engines 6 (2013) 400–421.

[9] C. Chartier, O. Andersson, B. Johansson, M. Musculus, M. Bobba, SAE International Journal of Engines 4 (2011) 1978–1992.

[10] H. Yun, R. D. Reitz, Journal of Engineering for Gas Turbines and Power 129 (2007) 279–286.

[11] R. Ehleskog, R. L. Ochoterena, SAE Technical Paper (2008).

[12] A. Sperl, SAE Technical Paper (2011).

[13] M. Bobba, M. Musculus, W. Neel, SAE International Journal of Engines 3 (2010) 496–516.

[14] A. Vanegas, H. Won, C. Felsch, M. Gauding, N. Peters, SAE Technical Paper (2008).

[15] Y. Hotta, M. Inayoshi, K. Nakakita, K. Fujiwara, I. Sakata, SAE Technical Paper (2005).

[16] D. Pierpont, D. Montgomery, R. D. Reitz, SAE Technical Paper (1995).

[17] C. Barro, F. Tschanz, P. Obrecht, K. Boulouchos, ASME Paper No. ICEF2012-92075 (2012).

[18] S. Molina, J. M. Desantes, A. Garcia, J. M. Pastor, SAE Technical Paper (2010).

[19] J. M. Desantes, J. Arrègle, J. J. López, A. García, SAE Technical Paper (2007).

[20] J. Arrègle, J. V. Pastor, J. J. López, A. García, Combustion and Flame 154 (2008) 448–461.

[21] E. C. N. www.sandia.gov/ECN (2015).

[22] A. A. Amsden, P. O'rourke, T. Butler, KIVA-II: A computer program for chemically reactive flows with sprays, Technical Report, Los Alamos National Lab., NM (USA), 1989.

[23] M. Jangi, R. Solsjo, B. Johansson, X.-S. Bai, International Journal of Heat and Fluid Flow 53 (2015) 68–80.

[24] G. DErrico, T. Lucchini, F. Contino, M. Jangi, X.-S. Bai, Combustion Theory and Modelling 18 (2014) 65–88.

[25] M. Jangi, T. Lucchini, G. DErrico, X.-S. Bai, Proceedings of the Combustion Institute 34 (2013) 3091–3098.

[26] T. Yao, Y. Pei, B.-J. Zhong, S. Som, T. Lu, K. H. Luo, Fuel 191 (2017) 339–349.

[27] S. Skeen, J. Manin, L. M. Pickett, SAE International Journal of Engines 8 (2015) 696–715.

[28] D. L. Siebers, SAE technical paper (1998).

[29] A. Hadadpour, X.-S. Bai, M. Jangi, in: Tenth Mediterranean Combustion Symposium.

[30] C. Chartier, U. Aronsson, Ö. Andersson, R. Egnell, R. Collin, H. Seyfried, M. Richter, M. Aldén, SAE Technical Paper (2009).

[31] C. A. Idicheria, L. M. Pickett, SAE Technical Paper (2006).

[32] J. E. Dec, Proceedings of the combustion institute 32 (2009) 2727–2742.

[33] M. P. Musculus, Journal of Fluid Mechanics 638 (2009) 117–140.